

Collinear scattering and long-time dynamical memory in two-dimensional electron fluids

Serhii Kryhin, Leonid Levitov

Department of Physics, Massachusetts Institute of Technology, Cambridge, MA 02139

(Dated: August 4, 2022)

Two-dimensional Fermi liquids have long been conjectured to host exceptionally long-lived excitations that arise due to collinear scattering governed by phase-space constraints. We present a direct calculation, showing that the lifetimes of these excitations surpass the fundamental bound set by Landau’s Fermi-liquid theory by a factor as large as $(T_F/T)^\alpha$ with $\alpha \approx 2$. To clarify this surprising behavior we connect quenching of Landau’s T^2 damping to dynamics of a fictitious quantum particle moving in a 1D supersymmetric reflectionless secant potential, obtained from a linearized quantum kinetic equation. In this framework, different long-lived excitations correspond to zero modes with different angular momenta. We identify new hydrodynamic modes arising due the long-lived excitations. Accordingly, 2D electron fluids feature new hydrodynamics with non-newtonian viscosity and several different viscous modes not anticipated by previous work.

Recent years have seen the advent of hydrodynamics as a framework to describe transport in quantum materials at diverse length and time scales [1–15]. However, despite this interest, the fundamental question of how an orderly hydrodynamic behavior on macroscales stems from a chaotic dynamics due to interactions and collisions on microscales, in particular the role of the quantum effects, has received relatively little attention. The situation is well understood for classical gases, where all moments of momentum distribution not protected by conservation laws are extremely fragile, being quickly erased after just a few (~ 1) collisions [16]. To the contrary, as shown below, quantum gases and liquids feature surprising collective memory effects occurring over the span of $N \gg 1$ collisions with N rapidly diverging at low temperatures.

Collective memory effects are particularly striking in two-dimensional (2D) systems that are at the center of ongoing efforts to achieve electron hydrodynamics [17–21]. The properties of 2D systems lie somewhere between those of 3D and 1D systems and are sharply distinct from both. For 3D systems, the theory of Fermi-liquids confirms Boltzmann’s short-time memory behavior with the onset of hydrodynamics occurring after ~ 1 collisions between quasiparticles [22]. The 1D systems feature manifestly non-Boltzmann behavior, described by the Luttinger-liquid theory that predicts integrable non-ergodic behavior that extends to arbitrarily large times and distances [23]. The unique behavior in 2D Fermi systems, which is due to the dominant role of head-on collisions and abnormally long-lived odd-parity momentum excitations [24–26], deviates strongly from that in both 3D and 1D systems.

The new long-lived excitations and collective modes are associated with odd-parity harmonics of the momentum distribution. The microscopic analysis of quasiparticle scattering at a 2D circular Fermi surface (FS), presented below, shows that for the odd-parity modes the Landau T^2 damping is quenched. Different excitations in this system are associated with different angular harmonics of FS modulations evolving in space and time as $\delta f(\mathbf{p}, \mathbf{x}, t) \sim \sum_m \alpha_m(\epsilon, \mathbf{x}, t) \cos m\theta + \beta_m(\epsilon, \mathbf{x}, t) \sin m\theta$,

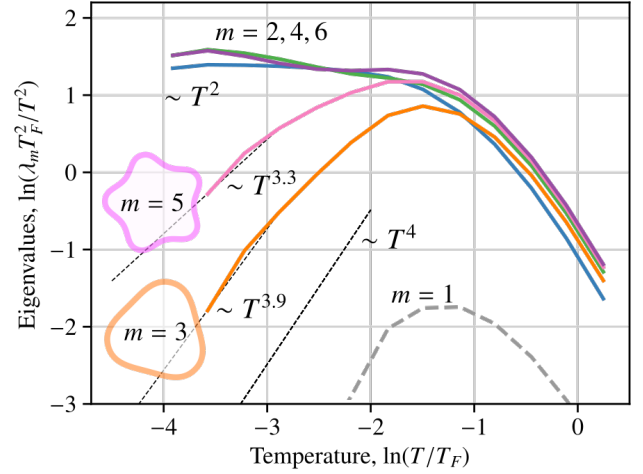


FIG. 1. Decay rates for different angular harmonics of particle distribution, scaled by T^2 , vs. temperature. Shown are dimensionless eigenvalues λ_m related to the decay rates through $\gamma_m = Ap_F^2 \lambda_m$, see Eq.34. Double-log scale is used to facilitate comparison of disparate time scales. Decay rates for even- m harmonics obey a T^2 scaling at $T \ll T_F$. Decay rates for odd- m harmonics are suppressed below those for even m and show “super-Fermi-liquid” scaling strongly deviating from T^2 . Odd- m decay rates can be approximated as T^α with $\alpha > 2$. An even/odd asymmetry in the rates and the suppression of decays for odd- m harmonics is seen already at $T \lesssim 0.16T_F$.

where θ is the angle parameterizing the FS. The microscopic decay rates, illustrated in Fig.1, govern dynamics of spatially-uniform excitations, $\alpha_m, \beta_m \sim e^{-\gamma_m t}$. As illustrated in Fig.1, at low temperatures $T \ll T_F$ the lifetimes of these modes greatly exceed the even-parity ones and show strong departure from conventional scaling. The decay rates in Fig.1 are obtained by a direct calculation that treats quasiparticle scattering exactly, using a method that does not rely on the small parameter $T/T_F \ll 1$. The odd- m decay rates display scaling $\gamma \sim T^\alpha$ with super-Fermi-liquid exponents $\alpha > 2$. In our analysis we find α values close to 4, i.e. the odd- m rates are suppressed strongly compared to the even- m rates,

$$\gamma_{\text{odd}}/\gamma_{\text{even}} \sim (T/T_F)^2.$$

This defines a new hierarchy of lifetimes for collective modes, leading to hydrodynamics with non-newtonian (scale-dependent) viscosity. To illustrate these properties we retain the two harmonics with longest lifetimes, $m = 1$ and 3 , and suppress those with other m . The velocity mode $m = 1$ is genuinely undamped owing to momentum conservation in two-body collisions, whereas the $m = 3$ mode represents the longest-lived odd-parity excitation (see Fig.1). Here we focus on the shear modes relevant for hydrodynamics, $\beta_1(\mathbf{x}, t) \sin \theta + \beta_3(\mathbf{x}, t) \sin 3\theta$, with θ measured from \mathbf{k} direction, with a harmonic dependence $\beta_m(\mathbf{x}, t) \sim e^{i\mathbf{k}\mathbf{x} - i\omega t}$. Integrating out the fast-relaxing modes with $m \neq 1, 3$ (see Supplement) yields a pair of coupled diffusion equations

$$\partial_t \beta_1 = -\nu k^2 \beta_1 - \nu k^2 \beta_3, \quad \partial_t \beta_3 = -(2\nu k^2 + \gamma_3) \beta_3 - \nu k^2 \beta_1$$

where $\nu = v_F^2/4\gamma_2$ is the ordinary ‘newtonian’ viscosity. These relations describe behavior at times and distances

$$\omega, kv_F \ll \gamma_{m \neq 1,3}.$$

Since $\gamma_3 \ll \gamma_{m \neq 1,3}$, we find two different hydrodynamic regimes, the short-time regime $\omega, \nu k^2 \gg \gamma_3$ and the long-time regime $\omega, \nu k^2 \ll \gamma_3$. In the first regime, i.e. at relatively short times $t\gamma_3 \ll 1$, these coupled modes yield two separate viscous modes found by diagonalizing the 2×2 problem, with viscosity taking universal values

$$\nu_1 = \frac{3 + \sqrt{5}}{2} \nu, \quad \nu_2 = \frac{3 - \sqrt{5}}{2} \nu \quad (1)$$

with a large ratio $\nu_1/\nu_2 = (3 + \sqrt{5})/(3 - \sqrt{5}) \approx 6.9$.

To gain insight in the behavior at long times, for which the memory effects matter, we eliminate the β_3 variable and write the dynamics in a closed form for the velocity mode. This yields Stokes equation with a scale-dependent (non-newtonian) viscosity:

$$-i\omega \beta_1 = \Xi(k, \omega) k^2 \beta_1, \quad \Xi(k, \omega) = \nu \frac{\nu k^2 + \gamma_3 - i\omega}{2\nu k^2 + \gamma_3 - i\omega}. \quad (2)$$

As expected, the newtonian viscosity $\Xi = \nu$ is recovered in the limit $kv, \omega \rightarrow 0$, whereas for $\nu k^2, \omega \gg \gamma_3$ Eq.(2) yields the two viscous modes found in Eq.(1).

The conventional (newtonian) hydrodynamics is restored at times and distances such that ω and νk^2 are smaller than γ_3 , i.e.

$$T > T_* = \frac{1}{\sqrt{2\gamma_2\gamma_3}}, \quad L > v_F T_*.$$

These lengthscales and timescales are reached by particles after undergoing about

$$N = T_* \gamma_2 = \sqrt{\frac{\gamma_2}{2\gamma_3}} \sim \frac{T_F}{T} \gg 1$$

collisions. The number of collisions required for the memory of the microstate to be erased diverges at $T \rightarrow 0$, indicating a sharply non-Boltzmann behavior.

It is instructive to note that the quenching of Landau’s T^2 damping for odd- m modes apparently contradicts the well-known results for excitation lifetimes in 2D Fermi gases found from Green’s function selfenergy calculations, which predict that collinear scattering shortens quasiparticle lifetimes[30–36]. Namely, decay rates predicted in this way are faster by a log factor $\log(T_F/T)$ than the conventional T^2 rates. The selfenergy approach is therefore conspicuously unaware of the existence of the long-lived odd- m excitations. This may seem surprising also because it is usually taken for granted that there is a single timescale that characterizes decay for all low-energy excitations. However, as made clear by Fig.1, this is very much untrue in 2D, since the odd- m and even- m modes have drastically different lifetimes that show different scaling vs. T . The conventional self-energy approach is not well suited for such a situation, since selfenergy is the quantity which is most sensitive to the fastest decay pathways. It is probably for this reason that the long-lived excitations, the main finding of the present work, have been missed in the literature despite the 60 years of intense interest in Fermi liquids.

We also emphasize that, similar to the self-energy analysis[30–36], the occurrence of long-lived excitations is a robust property that persists for non-circular Fermi surfaces, so long as the distortion away from the circle is not big. The reason is that the inversion symmetry, whenever present, separates modulations of the Fermi surface into modes of an even and odd parity. The difference in lifetimes for these mode types is identical to that found here for circular Fermi surfaces.

One more reason for why the long-lived modes have been missed in the literature undoubtedly lies in the difficulty of a direct calculation. To gain insight and understand better the origin of this difficulty we consider excitations at the Fermi surface in the framework of the Fermi-liquid kinetic equation. An approach developed in Refs.[22, 45–47] allows to tackle exactly the kinetic equation, linearized near thermal equilibrium at $T \ll T_F$, bringing it to the form of a time-dependent Schroedinger equation with a reflectionless secant potential. This equation, being exactly solvable, successfully predicts a T^2 scaling for excitation decay in 3D. However, it fails when applied in 2D, yielding unphysical vanishing rates.

To clarify the nature of long-lived modes we first demonstrate their relation with zero modes of the 1D quantum mechanics problem and, after that, present and discuss the results of a direct calculation. The starting point is the Fermi-liquid transport equation

$$\frac{df_1}{dt} + [f, H] = \sum_{21'2'} (w_{1'2' \rightarrow 12} - w_{12 \rightarrow 1'2'}), \quad (3)$$

where $f(\mathbf{p}, \mathbf{r}, t)$ is fermion distribution, $[f, H]$ denotes the Poisson bracket $\nabla_{\mathbf{r}} f \nabla_{\mathbf{p}} \epsilon - \nabla_{\mathbf{r}} \epsilon \nabla_{\mathbf{p}} f$. The right-hand side is the rate of change of the occupancy of a state \mathbf{p}_1 , given as a sum of the gain and loss contributions resulting from the two-body scattering processes $12 \rightarrow 1'2'$ and $1'2' \rightarrow$

12. Fermi's golden rule yields

$$w_{1'2' \rightarrow 12} = \frac{2\pi}{\hbar} |V_{12,1'2'}|^2 \delta_\epsilon \delta_{\mathbf{p}} (1 - f_1)(1 - f_2) f_{1'} f_{2'}, \quad (4)$$

where the delta functions $\delta_\epsilon = \delta(\epsilon_1 + \epsilon_2 - \epsilon_{1'} - \epsilon_{2'})$, $\delta_{\mathbf{p}} = \delta^{(2)}(\mathbf{p}_1 + \mathbf{p}_2 - \mathbf{p}_{1'} - \mathbf{p}_{2'})$ account for the energy and momentum conservation. The gain and loss contributions are related by the reciprocity symmetry $12 \leftrightarrow 1'2'$. Here $V_{12,1'2'}$ is the two-body interaction, properly antisymmetrized to account for Fermi statistics. Interaction $V_{12,1'2'}$ depends on momentum transfer k on the $k \sim k_F$ scale; this k dependence is inessential and will be ignored. In what follows we consider a spatially uniform problem setting $[f, H] = 0$. The sum over momenta $2, 1', 2'$ represents a six-dimensional integral over $\mathbf{p}_2, \mathbf{p}_{1'}$ and $\mathbf{p}_{2'}$, which is discussed below.

For the states weakly perturbed away from equilibrium, (4) can be linearized using the standard ansatz $f(\mathbf{p}) = f_0(\mathbf{p}) - \frac{\partial f_0}{\partial \epsilon} \eta(\mathbf{p})$. After standard algebra, this yields a linear integro-differential equation

$$f_0(1 - f_0) \frac{d\eta_1}{dt} = I_{ee} \eta, \quad (5)$$

$$I_{ee} \eta = \sum_{21'2'} \frac{2\pi}{\hbar} |V|^2 F_{121'2'} \delta_\epsilon \delta_{\mathbf{p}} (\eta_{1'} + \eta_{2'} - \eta_1 - \eta_2)$$

Here $\sum_{21'2'}$ and $|V|^2$ denote the six-dimensional integral $\int \frac{d^2 p_2 d^2 p_{1'} d^2 p_{2'}}{(2\pi)^6}$ and the interaction matrix element $|V_{12,1'2'}|^2$, the quantity $F_{121'2'}$ is a product of the equilibrium Fermi functions $f_1^0 f_2^0 (1 - f_{1'}^0)(1 - f_{2'}^0)$.

Different excitations are described by eigenfunctions of the collision operator I_{ee} , with the eigenvalues giving the decay rates equal to inverse lifetimes. Because of the cylindrical symmetry of the problem, the eigenfunctions are products of angular harmonics on the Fermi surface and functions of the radial energy variables $x_i = \beta(\epsilon - \mu)$:

$$\eta(\mathbf{p}, t) = e^{-\gamma_m t} e^{im\theta} \chi_m(x), \quad (6)$$

where γ_m and $\chi_m(x)$ are solutions of a spectral problem $-\gamma_m f_0(1 - f_0) \chi_m(x) = I_{ee} \chi_m(x)$.

In general, the six-dimensional integral operator I_{ee} has a complicated structure which is difficult to analyze. However, at $T \ll T_F$ the part of phase space in which transitions $12 \leftrightarrow 1'2'$ are not restricted by fermion exclusion is a thin annulus of radius p_F and a small thickness $\delta p \approx T/v \ll p_F$. One can therefore factorize the six-dimensional integration over $\mathbf{p}_2, \mathbf{p}_{1'}$ and $\mathbf{p}_{2'}$ in I_{ee} into a three-dimensional energy integral and a three-dimensional angular integral, and integrate over angles to obtain a close-form equation for the radial dependence $\chi(x)$. This is done by noting that the delta functions $\delta_\epsilon \delta_{\mathbf{p}}$ together with the conditions $|\mathbf{p}_1| \approx |\mathbf{p}_2| \approx |\mathbf{p}_{1'}| \approx |\mathbf{p}_{2'}| \approx p_F$ imply that the states $1, 2, 1'$ and $2'$ form two anti-collinear pairs

$$\mathbf{p}_1 + \mathbf{p}_2 \approx 0, \quad \mathbf{p}_{1'} + \mathbf{p}_{2'} \approx 0 \quad (7)$$

The azimuthal angles therefore obey $\theta_1 \approx \theta_2 + \pi$, $\theta_{1'} \approx \theta_{2'} + \pi$. In a thin-shell approximation $\delta p \ll p_F$, this gives two delta functions $\delta(\theta_1 - \theta_2 - \pi)$, $\delta(\theta_{1'} - \theta_{2'} - \pi)$ that cancel two out of three angle integrals in I_{ee} , allowing to rewrite the quantity $\eta_{1'} + \eta_{2'} - \eta_1 - \eta_2$ as

$$e^{im\theta_{1'}} (\chi(x_{1'}) + (-)^m \chi(x_{2'})) - e^{im\theta_1} (\chi(x_1) + (-)^m \chi(x_2)). \quad (8)$$

Subsequent steps differ for even and odd m , because the contributions of $\chi(x_{1'})$ and $\chi(x_{2'})$ to I_{ee} cancel out for odd m and double for even m , since F is symmetric in $x_{1'}$ and $x_{2'}$. Focusing on odd m and carrying out integration over the angle between \mathbf{p}_1 and $\mathbf{p}_{1'}$ yields

$$\tilde{F} \frac{d\chi(x_1)}{dt} = T^2 \int dx_2 dx_{1'} dx_{2'} F g \delta_x [\chi(x_1) - \chi(x_2)], \quad (9)$$

where $\tilde{F} = f_0(1 - f_0)$ and $\delta_x = \delta(x_1 + x_2 - x_{1'} - x_{2'})$. Here T^2 originates from nondimensionalizing the energy variables x_i in the integral and the delta function, the dimensionless factor g is a result of angular integration, the quantity F is defined above. Integration over energy variables $x_2, x_{1'}, x_{2'}$ extends throughout $-\infty < x_i < \infty$, as appropriate for $T \ll T_F$.

This equation, after introducing new distribution as $\chi(x) = 2 \cosh \frac{x}{2} \zeta(x)$ and carrying out Fourier transform in the energy variable, $\zeta(x) = \int dk e^{ikx} \psi(k)$, can be rewritten as a time-dependent Schroedinger equation for a particle moving in a one-dimensional secant potential

$$\partial_t \psi(k) = g T^2 \left[\left(\frac{\pi^2}{2} - \frac{\pi^2}{\cosh^2 \pi k} \right) \psi(k) - \frac{1}{2} \psi''(k) \right] \quad (10)$$

(see Supplement). Unlike the 3D case, where after a similar transformation the T^2 scaling translates into a T^2 dependence of the decay rates, here the operator in (10) has a zero mode, $\psi_0(k) = \frac{1}{\cosh(\pi k)}$. Being a zero mode, this mode does not relax. The associated $\chi_0(x)$ can be found from the identity $\int d\xi \frac{e^{2\pi i \xi y}}{\cosh \pi \xi} = \frac{1}{\cosh \pi y}$, giving $\chi_0(x) = 1$. Returning to the energy variable, this yields the Fermi-surface-displacement mode $\delta f(x) = df_0/dx = f_0(1 - f_0)$, identical for all odd m .

For even m , analysis proceeds in a similar manner, however it yields a normal T^2 scaling of the decay rates. This is so because for even m different terms in (8) are of equal signs and do not cancel out. As a result, the even- m and odd- m harmonics show a very different behavior. While the odd- m rates vanish in the zero-thickness approximation for the active shell at the Fermi surface, the even- m rates remain finite in this limit, scaling as T^2 . Infinite lifetimes found for odd- m modes indicate that the problem of lifetimes is too subtle to be successfully tackled by the 1D quantum mechanics approach.

This motivates us to attempt a direct calculation through diagonalizing the linearized collision operator I_{ee} without invoking the zero-thickness assumption $T \ll T_F$. This problem proves to be quite demanding for several reasons. First, the eigenstates of I_{ee} are localized in a peculiar phase space region, an annulus at the Fermi surface

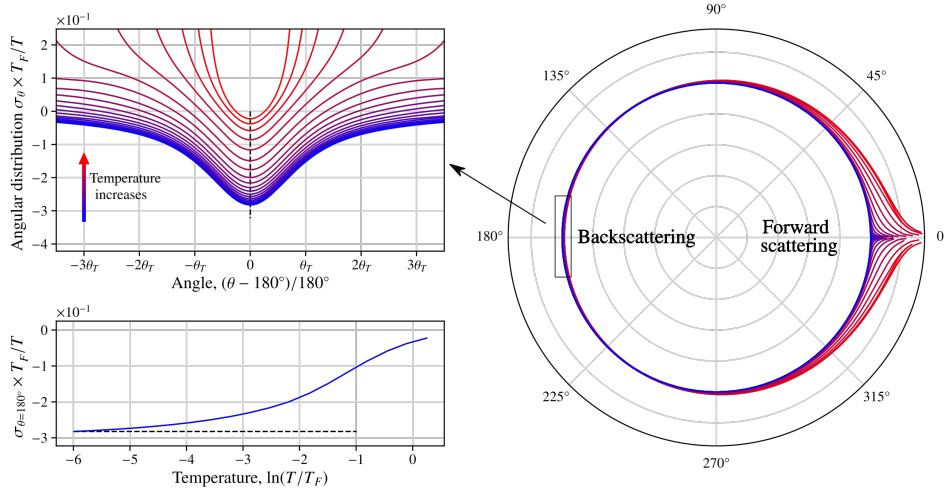


FIG. 2. a) Angular distribution $\sigma(\theta)$ for the two-body process of quasiparticle scattering, (11), at different temperatures. Restricted phase space gives rise to collinear scattering, producing sharp peaks in the forward and backward directions, $\theta = 0$ and π . b),c) The back-scattering peak shows a $\sim T^2$ scaling of the intensity and a $\sim T$ scaling of peak width. Temperature values used: $T/T_F = 0.0025, 0.005, 0.01, 0.02, 0.04, 0.08, 0.16, 0.32, 0.64, 1.28$.

of width proportional to T . Sampling this “active part” of p space requires a mesh which is adjusted with temperature. Second, capturing the kinematic constraints that lead to collinear collision effects, requires “high-fines” sampling of the near-collinear momenta as compared to the generic momenta in the annulus. Things are made still more complex by the fact that the angular width of the active collinear region also varies with temperature, decreasing as T [see Supplement for details]. To tackle this problem, we make use of the cylindrical symmetry of our system and link the decay rates for different modes to the angular distribution for scattering induced by a test particle injected in the system. Computing the angular distribution as described below, we Fourier-transform it in θ to find decay rates for individual modes. This scheme allows us to directly diagonalize the collision operator, Eq.(5), finding the results shown in Fig.1.

The angular distribution of particles scattered after a test particle has been injected in the system at an energy near the Fermi level, $f_i(\theta) = J_0\delta(\theta - \theta_i)$, is given by

$$f(\theta) = \oint \frac{d\theta'}{2\pi} \sigma(\theta - \theta') f_i(\theta') = \frac{J_0}{2\pi} \sigma(\theta - \theta_i), \quad (11)$$

where $f_i(\theta)$ describes the injected beam and the scattering angle θ parameterizes the Fermi surface. Here J_0 is a T -independent intensity of the injected beam and, for simplicity, we suppressed the width of the distribution in the radial direction. As discussed above, excitations with different lifetimes are represented as normal modes of the two-body collision operator linearized in the deviation of the distribution from the equilibrium state $I f_m(\theta) = -\gamma_m f_m(\theta)$, where γ_m are the decay rates (inverse lifetimes) for different excitations. Due to the cylindrical symmetry of the problem, the normal modes are the angular harmonics $f_m(\theta) = e^{im\theta}$ times some functions of the radial momentum variable that we ignore

for the moment. Comparing to Eq.11 we see that the quantities γ_m are related to the Fourier coefficients of the angular distribution,

$$\sigma(\theta) = \sum_m e^{im(\theta - \theta_i)} (\gamma_m - \gamma_0), \quad (12)$$

where the term $-\gamma_0$ describes particle loss from the injected beam. We use the basis functions introduced above to compute $\sigma(\theta)$ and then use the relation in (12) to obtain lifetimes of different modes.

The angular dependence, shown in Fig.2, features sharp peaks centered at $\theta = 0$ and π , describing forward scattering and backscattering, respectively. The angular widths θ_T of the peaks scale as T at $T \ll T_F$. Notably, the backscattering peak is of a negative sign, representing backreflected holes. At $T \ll T_F$ the values $\sigma(\theta)$ at generic θ within the peak scale as T . Multiplying this by the peak width $\theta_T \sim T/T_F$ yields the net backscattering rate that scales as T^2/T_F , as expected from Fermi-liquid theory. This behavior is detailed in Fig.2 insets.

The decay rates γ_m for odd- m modes, found from the relation in (12), show significant departure from the T^2 scaling. The decay rates for harmonics $e^{im\theta}$ with even and odd m , shown in Fig.1, are similar at $T \sim T_F$ but show a very different behavior at $T < T_F$. This difference between even- m and odd- m rates originates from the collinear character of scattering, manifest in the strong peaks in $\sigma(\theta)$ in the forward and backward directions. The nearly equal areas of these peaks and the negative sign of the backscattering peak suppress the odd- m Fourier harmonics of $\sigma(\theta)$, giving small decay rates for these harmonics. The temperature dependence for the even- m harmonics agrees well with the T^2 law. The odd- m harmonics, to the contrary, have decay rates decreasing at low T much faster than T^2 . For these harmonics, the observed scaling is $\gamma_m \sim T^\alpha$ with α slightly below

4. This represents a “super-Fermi-liquid” suppression of the decay rates for odd- m harmonics.

Lastly, it is interesting to mention that collinear scattering, manifest in the sharp peaks in the angle-resolved cross-section $\sigma(\theta)$ at $\theta = 0$ and π , is directly responsible for the log enhancement of quasiparticle decay rates predicted from the self-energy analysis. Indeed the angle dependence near $\theta = 0$ and π is of the form $\sigma(\theta) \sim T^2/|\theta|$ and $T^2/|\theta - \pi|$, with the $1/|\theta|$ singularity rounded on the scale $\delta\theta \sim T/T_F$, as illustrated in Fig.2 (see above). Integrating the angle-resolved crosssection over θ yields a $\log(T_F/T)T^2$ total scattering crosssection.

This illustrates that the abnormally long lived excitations with the decay rates that scale as T^4 rather than T^2 , described in this work, and the seminal $\log(T_F/T)T^2$ decay rates, originate from the same phase-space constraints. Restricted phase space renders quasiparticle scattering a highly collinear process even when the microscopic interactions have a weak angular dependence.

The unusual kinetics originating in this regime, is relevant for a variety of 2D systems, in particular those where small carrier density and small kinetic energy make electron-electron collisions a dominant scattering mechanism that overwhelms other carrier relaxation pathways. These long-lived excitations manifest themselves through new hydrodynamic modes with non-newtonian (scale-dependent) viscosity. This leads to multiple viscous modes impossible in conventional fluids, providing a clear testable signature of the unique behavior originating from long-lived excitations in electron fluids.

We thank Dmitry Maslov for inspiring discussions and Rokas Veitas for assistance at the initial stages of this project. This work was supported by the Science and Technology Center for Integrated Quantum Materials, NSF Grant No. DMR1231319; Army Research Office Grant W911NF-18-1-0116; and Bose Foundation Research fellowship.

-
- [1] Müller, M., Schmalian, J., Fritz, L. Graphene: a nearly perfect fluid. *Phys. Rev. Lett.* 103, 2-5 (2009).
- [2] A. Tomadin, G. Vignale, M. Polini, A Corbino disk viscometer for 2D quantum electron liquids *Phys. Rev. Lett.* 113, 235901 (2014).
- [3] A. Principi, G. Vignale, M. Carrega, M. Polini, Bulk and shear viscosities of the two-dimensional electron liquid in a doped graphene sheet *Phys. Rev. B* 93, 125410 (2016)
- [4] Scaffidi, T., Nandi, N., Schmidt, B., Mackenzie, A. P., Moore, J. E. Hydrodynamic electron flow and Hall viscosity. *Phys. Rev. Lett.* 118, 226601 (2017).
- [5] A. Lucas, K. C. Fong, Hydrodynamics of electrons in graphene, *J. Phys.: Condens. Matter* 30 053001 (2018).
- [6] Guerrero-Becerra, K. A., Pellegrino, F. M. D., Polini, M. Magnetic hallmarks of viscous electron flow in graphene. *Phys. Rev. B* 99, 041407 (2019).
- [7] Narozhny, B. N., Sch’utt, M. Magnetohydrodynamics in graphene: Shear and Hall viscosities. *Phys. Rev. B* 100, 035125 (2019).
- [8] Alekseev, P. S., Dmitriev, A. P. Viscosity of two-dimensional electrons. *Phys. Rev. B* 102, 241409 (2020)
- [9] Toshio, R., Takasan, K., Kawakami, N. Anomalous hydrodynamic transport in interacting noncentrosymmetric metals. *Phys. Rev. Res.* 2, 032021 (2020).
- [10] Narozhny, B. N., Gornyi, I. V., Titov, M. Hydrodynamic collective modes in graphene. *Phys. Rev. B* 103, 115402 (2021).
- [11] Hasdeo, E. H., Ekström, J., Idrisov, E. G., Schmidt, T. L. Electron hydrodynamics of two-dimensional anomalous Hall materials. *Phys. Rev. B* 103, 125106 (2021).
- [12] M. Qi, A. Lucas, Distinguishing viscous, ballistic, and diffusive current flows in anisotropic metals, *Phys. Rev. B* 104 (19), 195106 (2021)
- [13] C. Q. Cook, A. Lucas, Viscometry of electron fluids from symmetry, *Phys. Rev. Lett.* 127 (17), 176603 (2021)
- [14] D. Valentinis, J. Zaanen, D. van der Marel Propagation of shear stress in strongly interacting metallic Fermi liquids enhances transmission of terahertz radiation *Sci. Rep.* 11, 7105 (2021)
- [15] D. Valentinis, Optical signatures of shear collective modes in strongly interacting Fermi liquids *Phys. Rev. Research* 3, 023076 (2021)
- [16] R. L. Liboff, *Kinetic Theory: Classical, Quantum, and Relativistic Descriptions* (Springer-Verlag, New York, 2003)
- [17] J. A. Sulpizio, L. Ella, A. Rozen, J. Birkbeck, D. J. Perello, D. Dutta, M. Ben-Shalom, T. Taniguchi, K. Watanabe, T. Holder, R. Queiroz, A. Principi, A. Stern, T. Scaffidi, A. K. Geim, S. Ilani, Visualizing Poiseuille flow of hydrodynamic electrons *Nature* 576, 75-79 (2019)
- [18] M. J. H. Ku, T. X. Zhou, Q. Li, Y. J. Shin, J. K. Shi, C. Burch, L. E. Anderson, A. T. Pierce, Y. Xie, A. Hamo, U. Vool, H. Zhang, F. Casola, T. Taniguchi, K. Watanabe, M. M. Fogler, P. Kim, A. Yacoby, R. L. Walsworth, Imaging viscous flow of the Dirac fluid in graphene *Nature* 583, 537-541 (2020)
- [19] B. A. Braem, F. M. D. Pellegrino, A. Principi, M. Roosli, C. Gold, S. Hannel, J. V. Koski, M. Berl, W. Dietsche, W. Wegscheider, M. Polini, T. Ihn, and K. Ensslin, Scanning gate microscopy in a viscous electron fluid *Phys. Rev. B* 98, 241304(R) (2018).
- [20] U. Vool, A. Hamo, G. Varnavides, Y. Wang, T. X. Zhou, N. Kumar, Y. Dovzhenko, Z. Qiu, C. A. C. Garcia, A. T. Pierce, J. Gooth, P. Anikeeva, C. Felser, P. Narang, A. Yacoby, Imaging phonon-mediated hydrodynamic flow in WTe2 *Nature Physics* 17, 1216-1220 (2021).
- [21] Direct observation of vortices in an electron fluid A. Aharon-Steinberg, T. V’olkl, A. Kaplan, A. K. Pariari, I. Roy, T. Holder, Y. Wolf, A. Y. Meltzer, Y. Myasoedov, M. E. Huber, B. Yan, G. Falkovich, L. S. Levitov, M. H’ucker, E. Zeldov *Nature* 607, 74-80 (2022).
- [22] G. Baym, C. Pethick, *Landau Fermi-Liquid Theory: Concepts and Applications* (Wiley, 1991)
- [23] T. Giamarchi, *Quantum Physics in One Dimension*, Clarendon Press, Oxford, 2004.
- [24] R. N. Gurzhi, A. N. Kalinenko, and A. I. Kopeliovich, Electron-Electron Collisions and a New Hydrodynamic Effect in Two-Dimensional Electron Gas, *Phys. Rev.*

- Lett. 74, 3872 (1995)
- [25] H. Buhmann, L. W. Molenkamp, 1D diffusion: a novel transport regime in narrow 2DEG channels, *Physica E* 12, 715-718 (2002)
- [26] P. J. Ledwith, H. Guo, L. Levitov, Angular Superdiffusion and Directional Memory in Two-Dimensional Electron Fluids, arXiv:1708.01915
- [27] P. Ledwith, H. Guo, A. Shytov, L. Levitov Tomographic Dynamics and Scale-Dependent Viscosity in 2D Electron Systems, *Phys. Rev. Lett.* 123, 116601 (2019)
- [28] P. J. Ledwith, H. Guo, L. Levitov, The Hierarchy of Excitation Lifetimes in Two-Dimensional Fermi Gases, *Ann. Phys.* 411, 167913 (2019)
- [29] G. Giuliani and G. Vignale, *Quantum Theory of the Electron Liquid* (Cambridge University Press, 2012)
- [30] C. Hodges, H. Smith, and J. W. Wilkins, Effect of Fermi Surface Geometry on Electron-Electron Scattering, *Phys. Rev. B* 4, 302 (1971).
- [31] A. V. Chaplik, Energy Spectrum and Electron Scattering Processes in Inversion Layers, *Zh. Eksp. Teor. Fiz.* 60, 1845-1852 (1971) [English translation - *Sov. Phys. JETP* 33, 997 (1971).]
- [32] P. Bloom, Two-dimensional Fermi gas, *Phys. Rev. B* 12, 125 (1975).
- [33] G. F. Giuliani and J. J. Quinn, Lifetime of a quasiparticle in a two-dimensional electron gas, *Phys. Rev. B* 26, 4421 (1982).
- [34] L. Zheng and S. Das Sarma, Coulomb scattering lifetime of a two-dimensional electron gas, *Phys. Rev. B* 53, 9964 (1996).
- [35] D. Menashe, B. Laikhtman, Quasiparticle lifetime in a two-dimensional electron system in the limit of low temperature and excitation energy, *Phys. Rev. B* 54, 11561 (1996)
- [36] A. V. Chubukov and D. L. Maslov, *Phys. Rev. B* 68, 155113 (2003).
- [37] J. González, F. Guinea, and M. A. H. Vozmediano, Unconventional Quasiparticle Lifetime in Graphite, *Phys. Rev. Lett.* 77, 3589 (1996)
- [38] D. Brida, A. Tomadin, C. Manzoni, Y. J. Kim, A. Lombardo, S. Milana, R. R. Nair, K. S. Novoselov, A. C. Ferrari, G. Cerullo, M. Polini, Ultrafast collinear scattering and carrier multiplication in graphene, *Nature Communications* 4, 1987 (2013)
- [39] J. C. W. Song, K. J. Tielrooij, F. H. L. Koppens, L. Levitov, Photoexcited carrier dynamics and impact-excitation cascade in graphene *Phys. Rev. B* 87, 155429 (2013)
- [40] Q. Li and S. Das Sarma, Finite temperature inelastic mean free path and quasiparticle lifetime in graphene *Phys. Rev. B* 87 085406 (2013)
- [41] U. Briskot, I. A. Dmitriev, and A. D. Mirlin, Relaxation of optically excited carriers in graphene: Anomalous diffusion and Lévy flights, *Phys. Rev. B* 89 075414 (2014)
- [42] M. Trushin, Collinear scattering of photoexcited carriers in graphene, *Phys. Rev. B* 94, 205306 (2016)
- [43] C. Lewandowski, L. Levitov, Photoexcitation cascade and quantum-relativistic jets in graphene, *Phys. Rev. Lett.* 120, 076601 (2018)
- [44] E. I. Kiselev and J. Schmalian, Lévy Flights and Hydrodynamic Superdiffusion on the Dirac Cone of Graphene, *Phys. Rev. Lett.* 123, 195302 (2019)
- [45] G. A. Brooker, J. Sykes, Transport Properties of a Fermi Liquid, *Phys. Rev. Lett.* 21, 279 (1968)
- [46] H. Hojgard Jensen, H. Smith, and J. Wilkins, *Phys. Lett. A* 27, 532 (1968).
- [47] J. Sykes, G. A. Brooker, The transport coefficients of a fermi liquid, *Ann. Phys. (N. Y.)* 56, 1-39 (1970)
- [48] *J. Math. Phys.* 52, 063301 (2011); <https://doi.org/10.1063/1.3598428> K. Kanki, S. Tanaka, and T. Petrosky, Kinetic equations for classical and quantum Brownian particles and eigenfunction expansions as generalized functions, *J. Math. Phys.* 52, 063301 (2011).

Supporting Material for “Collinear scattering and long-lived excitations at a 2D Fermi surface”

Non-newtonian hydrodynamics due to long-lived modes

Here we show that the long-lived excitations result in a peculiar hydrodynamics with scale-dependent (non-newtonian) viscosity. To that end, we consider the kinetic transport equation linearized near the equilibrium state,

$$(\partial_t + \mathbf{v} \cdot \nabla) \delta f - I[\delta f] = -e\mathbf{E}(r) \cdot \frac{\partial f_0}{\partial \mathbf{p}}, \quad (13)$$

where I is a linearized collision integral, \mathbf{E} is the electric field, and $\delta f(p, r, t) = f - f_0$ describes a state weakly perturbed away from the Fermi-Dirac equilibrium state $f_0(p) = 1/(e^{\beta(\epsilon(p) - \mu)} + 1)$.

Next, we carry out the Fourier transform,

$$\delta f(p, r, t) = \sum_{\mathbf{k}, \omega} \delta f(p) e^{i\mathbf{k}\mathbf{r} - i\omega t},$$

and, taking into account that the momentum distribution $\delta f(p)$ is concentrated near the Fermi surface, expand it in the angular harmonics basis:

$$\delta f(p) = -\frac{\partial f_0}{\partial p} \sum_m e^{-im\theta} \delta f_m. \quad (14)$$

where θ is the angle parameterizing the Fermi surface measured from the direction of \mathbf{k} . The angular harmonics diagonalize the collision integral $I[\delta f_m] = -\gamma_m \delta f_m$.

The electric field $\mathbf{E}(r)$ can be either applied externally, as required, for instance, for calculating conductivity, or can be internal to the system, describing the electron-electron interactions in the Fermi liquid. Focusing on the latter case, here we consider the electric field induced by the density perturbed away from equilibrium. For Fourier harmonics, this gives

$$\mathbf{E}(k) = -i\mathbf{k}U(\mathbf{k}) \sum_p \delta f(p), \quad U(\mathbf{k}) = \frac{2\pi e^2}{\kappa|\mathbf{k}|}, \quad (15)$$

where κ is the dielectric constant. Plugging $\mathbf{E}(k)$ in the Eq. (13) yields a system of coupled equations for different harmonics δf_m . This problem describe both longitudinal and transverse modes, where $\delta f_m = \delta f_{-m}$ and $\delta f_m = -\delta f_{-m}$, respectively. Here we focus on the transverse modes (therefore, assume that $\delta f_m = -\delta f_{-m}$) and show that the hybridization of the $m = \pm 1$ and $m = \pm 3$ harmonics results in modes with a scale-dependent (non-newtonian) viscosity. Since the condition for transverse modes, $\delta f_m = -\delta f_{-m}$, implies $\delta f_0 = 0$, the transverse modes are not accompanied by charge buildup. Accordingly, in this case the electric field drops out. The electric field term, however, is important for the longitudinal modes such as plasmons. With this in mind, we will write the kinetic equation in a general form which includes the \mathbf{E} term:

$$(\gamma_m - i\omega) \delta f_m + \frac{ikv}{2} (\delta f_{m-1} + \delta f_{m+1}) = -\frac{ievk}{2m} \frac{\partial f_0}{\partial \epsilon} U(k) \delta f_0 (\delta_{m,1} + \delta_{m,-1}), \quad (16)$$

where mode decay rates γ_m obey relations (i) $\gamma_0 = 0$ due to particle conservation, (ii) $\gamma_m = \gamma$ for $m \neq 1, 3$, and $\gamma_3 = \gamma' \ll \gamma$ for long-lived excitations. At sufficiently long times such that $\omega \ll \gamma$, the even- m harmonics are mostly relaxed, giving an expression that links the even harmonics to the odd harmonics:

$$\delta f_{2m} = -\frac{ikv}{2\gamma} (\delta f_{2m+1} + \delta f_{2m-1}). \quad (17)$$

For the odd- m harmonics we write separately the expressions for the $m = \pm 1$ and $m = \pm 3$ harmonics,

$$(\gamma_p - i\omega) \delta f_{\pm 1} + \frac{ikv}{2} (\delta f_0 + \delta f_{\pm 2}) = -\frac{ievk}{2m} U(k) \frac{\partial f_0}{\partial \epsilon} \delta f_0 \quad (18)$$

$$(\gamma' - i\omega) \delta f_{\pm 3} + \frac{ikv}{2} (\delta f_{\pm 2} + \delta f_{\pm 4}) = 0 \quad (19)$$

The above equations are true for both the transverse and longitudinal modes.

From now on we specialize to transverse modes. In this case, as noted above, density remains unperturbed, $\delta f_0 = 0$, and therefore the electric field \mathbf{E} induced by density variation, Eq.(15), vanishes. Introducing notation $\nu = v^2/4\gamma$ and plugging Eqs.(17) and (19) into Eq. (18), and solving for the velocity mode $m = 1$, we obtain a collective mode dispersion relation

$$\gamma_p - i\omega + \nu k^2 - \frac{(\nu k^2)^2}{\gamma' - i\omega + 2\nu k^2} = 0. \quad (20)$$

This relation, compared to the one defined by the Stokes equation, $-i\omega + \gamma_p + \nu k^2 = 0$, indicates that our system is described by a scale-dependent viscosity, as discussed in the main text,

$$\Xi(\omega, k) = \nu \frac{\gamma' - i\omega + \nu k^2}{\gamma' - i\omega + 2\nu k^2}$$

In the limit $\gamma_p = 0$ and $|\omega| \ll \gamma'$, this predicts a non-newtonian viscous mode of the form $i\omega = \tilde{\nu}k^2$, where

$$\tilde{\nu} = \nu \left(1 - \frac{\nu k^2}{\gamma'} \right), \quad (21)$$

and one slowly-decaying mode with $i\omega \sim \gamma'$. In the limit $\gamma' \ll |\omega| \ll \gamma$, we obtain two viscous modes with different viscosities

$$\tilde{\nu}_{1,2} = \frac{3 \pm \sqrt{5}}{2} \nu \quad (22)$$

with a universal ratio $\nu_1/\nu_2 = (3 + \sqrt{5})/(3 - \sqrt{5})$. As a sanity check, in the limit when the long-lived mode becomes short-lived, $\gamma' \approx \gamma$, only one (the ordinary newtonian) viscous mode survives.

Since the number of the viscous modes changes with the scale, it is instructive to track the transformation of each mode with k . Eq.(20) yields a quadratic equation that can be solved to obtain two distinct dispersing modes:

$$i\omega = \frac{1}{2} (\gamma_p + \gamma' + 3\nu k^2) \pm \sqrt{(\nu k^2)^2 + \frac{1}{4} (\gamma' - \gamma_p + \nu k^2)^2}. \quad (23)$$

From this result we can recover all asymptotic regimes discussed above. In the long-wavelength limit $\nu k^2 \ll \gamma'$, one of the modes indeed remains damped, with $i\omega$ proportional to γ' (assuming $\gamma_p \ll \gamma'$). The second mode in this limit is viscous and has viscosity described by Eq.(21). The viscous mode in Eq.(21) upon varying k transforms into the mode $\tilde{\nu}_2$ in Eq.(22) with a minus sign.

This provides a simple illustration of a relation between the long-lived excitations and novel hydrodynamic effects, such as scale-dependent viscosity and, at intermediate times and distances, multiple viscous modes with different viscosity values. It is all but natural to expect that this behavior persists when more long-lived excitation modes are present in the system.

Transforming the collision integral to the partial differential equation

In this section we show the transformation of the collision integral into a second order partial differential equation, which can be carried out after the integration over angles is separated from the integration over energies.

As a first step, we reverse signs of the 1' and 2' variables: $x_{1'} \rightarrow -x_{1'}$, $x_{2'} \rightarrow -x_{2'}$. This transforms the integral equation (9) to

$$\begin{aligned} \tilde{F} \frac{d\chi}{dt} &= gT^2 \int dx_2 dx_1' dx_2' F_{121'2'} \delta_x^+ (\chi(x_1) - \chi(x_2)), \\ F_{121'2'} &= f_0(x_1) f_0(x_2) f_0(x_{1'}) f_0(x_{2'}) \end{aligned} \quad (24)$$

where $\delta_x^+ = \delta(x_1 + x_2 + x_{1'} + x_{2'})$. Next we use the identities

$$\int dx_2 dx_1' dx_2' f_0(x_2) f_0(x_{1'}) f_0(x_{2'}) \delta_x^+ = \frac{1}{2} \frac{x_1^2 + \pi^2}{1 + e^{-x_1}}, \quad (25)$$

$$\int dx_1' dx_2' f_0(x_{1'}) f_0(x_{2'}) \delta_x^+ = -\frac{x_1 + x_2}{1 - e^{-x_1 - x_2}} \quad (26)$$

to carry out integration over x_2, x_1', x_2' in the first term and over x_1', x_2' in the second term. This brings the integral equation to the form

$$\tilde{F} \frac{d\chi}{dt} = gT^2 \left[f_0(x_1) \frac{1}{2} \frac{x_1^2 + \pi^2}{1 + e^{-x_1}} \chi(x_1) \right. \quad (27)$$

$$\left. + \int dx_2 f_0(x_1) f_0(x_2) \frac{x_1 + x_2}{1 - e^{-x_1 - x_2}} \chi(x_2) \right] \quad (28)$$

This equation can be simplified using the substitution

$$\chi(x) = 2 \cosh\left(\frac{x}{2}\right) \zeta(x) = \left(e^{x/2} + e^{-x/2}\right) \zeta(x), \quad (29)$$

which gives an equation

$$\frac{d\zeta(x_1)}{dt} = gT^2 \left[\frac{x_1^2 + \pi^2}{2} \zeta(x_1) + \int dx_2 \frac{x_1 + x_2}{2 \sinh \frac{x_1 + x_2}{2}} \zeta(x_2) \right]$$

Next, we reverse the sign of x_2 , which brings the integral operator to the form of a convolution, separately for the even and odd functions $\zeta(x_2)$. For an even function $\zeta(-x_2) = \zeta(x_2)$ we have

$$\int dx_2 \frac{x_1 - x_2}{2 \sinh \frac{x_1 - x_2}{2}} \zeta(x_2).$$

After Fourier transform $\zeta(x) = \int dk e^{ikx} \psi(k)$ this gives the time-dependent Schroedinger equation with a secant potential $\frac{\pi^2}{\cosh^2 \pi k}$ displayed in the main text, (30). Physical solutions correspond to the eigenfunctions that are even in k . The zero mode $\psi_0(k) = \frac{1}{\cosh(\pi k)}$, being an even function of k , is part of this family. Going back to the x variable and undoing the substitutions gives the zero mode $\chi_0(x) = 1$ for all odd m , and $\delta f_0(x) = f_0(x)(1 - f_0(x))$ as discussed in the main text.

Analogously, for odd functions $\zeta(-x_2) = -\zeta(x_2)$ upon changing x_2 to $-x_2$ a minus sign appears in front of the integral operator:

$$- \int dx_2 \frac{x_1 - x_2}{2 \sinh \frac{x_1 - x_2}{2}} \zeta(x_2).$$

Carrying out Fourier transform $\zeta(x) = \int dk e^{ikx} \psi(k)$ give a time-dependent Schroedinger equation for a particle moving in a secant potential of an opposite sign

$$\partial_t \psi(k) = gT^2 \left[\left(\frac{\pi^2}{2} + \frac{\pi^2}{\cosh^2 \pi k} \right) \psi(k) - \frac{1}{2} \psi''(k) \right] \quad (30)$$

In this case, physical solutions correspond to the eigenfunctions that are odd in k . For a repulsive secant potential these functions are in the continuum spectrum and asymptotically have the form of plane waves. This indicates that the behavior of the eigenfunctions that are odd in x differs from that of the even eigenfunctions discussed above. This poses interesting questions for future work.

Direct diagonalization of the linearized collision operator: an overview

Here we proceed in two steps, first using the kinematic constraints to reduce the six-dimensional integral in (5) to a three-dimensional integral, and then using a suitable basis of functions to reduce the three-dimensional integrals to one-dimensional integrals. After that, the operator I_{ee} can be projected on a subspace that represents adequately the states on the active shell and diagonalized numerically.

Integration over \mathbf{p}_2 can be eliminated by a momentum-conservation delta-function, giving

$$I[\eta] = -\frac{2\pi}{\hbar} |V|^2 \int \frac{d^2 p_1' d^2 p_2'}{(2\pi)^4} F_{121'2'} \delta_\epsilon \cdot \sum_\alpha' \eta_\alpha, \quad (31)$$

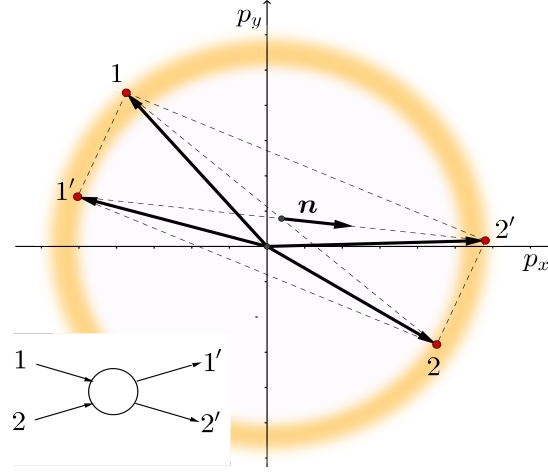


FIG. 3. Ingoing and outgoing momenta that contribute to excitation dynamics for a typical scattering processes $12 \rightarrow 1'2'$ shown in the inset. The blurred annulus of radius $p = p_F$ and width $\delta p \sim T/v$ is the region near the Fermi surface where collisions are allowed by fermion exclusion. Kinematic constraints select processes in which momenta form nearly anticollinear pairs 1-2 and $1'-2'$, see (7). Shown is the vector \mathbf{n} , (33), used to parameterize momentum states, $\mathbf{n} = \frac{\mathbf{p}_{2'} - \mathbf{p}_{1'}}{|\mathbf{p}_{2'} - \mathbf{p}_{1'}|} = (\cos \theta_n, \sin \theta_n)$.

where \mathbf{p}_2 is now a function of the other momenta, $\mathbf{p}_2 = \mathbf{p}_{1'} + \mathbf{p}_{2'} - \mathbf{p}_1$. As above, δ_ϵ denotes $\delta(\epsilon_1 + \epsilon_2 - \epsilon_{1'} - \epsilon_{2'})$ and $\sum'_\alpha \eta_\alpha$ stands for $\eta_{1'} + \eta_{2'} - \eta_1 - \eta_2$. Next, we eliminate the radial integration over $|\mathbf{p}_{2'}|$ by canceling it with the energy delta-function. The expression for the collision integral then takes the form

$$I[\eta] = -A \int \frac{d^2 p_2 d\theta_n}{(2\pi)^4} F_{121'2'} \sum'_\alpha \eta_\alpha, \quad A = \pi m |V|^2 / \hbar^3, \quad (32)$$

where we introduced an angle θ_n defined through the kinematic relation between the incoming and outgoing momenta as follows. Due to momentum and energy conservation, in (32) the momenta $\mathbf{p}_{1'}$ and $\mathbf{p}_{2'}$ satisfy the constraints

$$\mathbf{p}_{1'} = \mathbf{p}_+ + |\mathbf{p}_-| \mathbf{n}, \quad \mathbf{p}_{2'} = \mathbf{p}_+ - |\mathbf{p}_-| \mathbf{n}, \quad (33)$$

where $\mathbf{p}_\pm = \frac{\mathbf{p}_1 \pm \mathbf{p}_2}{2}$ and we introduced a unit vector $\mathbf{n} = (\cos \theta_n, \sin \theta_n)$ that parameterizes the outgoing momenta in the collision process, wherein the incoming momenta \mathbf{p}_1 and \mathbf{p}_2 are taken to be fixed, see schematic in Fig.3.

The temperature-independent constant A defined in Eq.32, which describes the scattering potential strength, can be used to non-dimensionalize the decay rates for different excitations, γ_m . Namely, γ_m are related to the eigenvalues λ_m of the dimensionless linear integral operator introduced in the main text and analyzed below as

$$\gamma_m = A p_F^2 \lambda_m \quad (34)$$

(as a reminder, p_F denotes the Fermi wavevector rather than the Fermi momentum, and thus has units 1/length). This relation can be used to relate λ_m values shown in Fig.1 of the main text with physical decay rates.

Next, we choose a basis of functions to represent the states $\eta(\mathbf{p}_1)$ and define a matrix representation for the linear operator $I[\eta_{\mathbf{p}_1}]$. Different choices of basis functions have different computational limitations. Here we employ, as a basis, the δ -functions

$$\eta_{\mathbf{k}}(\mathbf{p}) = \delta^{(2)}(\mathbf{p} - \mathbf{k}) \quad (35)$$

labeled by different \mathbf{k} [for a discussion of normalization, which depends on the choice of the mesh, see Supplement] This basis combines computational efficiency with analytic simplicity. Indeed, the two-dimensional delta functions, (35), when substituted in the collision operator, cancel two out of three integrations in $\int dp_2 d\theta_2 d\theta_n \dots$ yielding an expression that involves just one integral.

An added benefit of working in the delta-function basis is that it allows to analytically simplify the expression for the collision operator, (32). The collision operator can be written as a sum of four contributions, one for each η_α . This yields an expression $I[\eta] = I_1[\eta] + I_2[\eta] - I_3[\eta] - I_4[\eta]$ with the individual terms given below:

$$I_1[\eta_{\mathbf{k}}] = -A \eta_{\mathbf{k}}(\mathbf{p}_1) \int \frac{d^2 p_2 d\theta_n}{(2\pi)^4} F_{121'2'}, \quad (36)$$

$$I_2[\eta_{\mathbf{k}}] = -A \int \frac{d\theta_n}{(2\pi)^4} F_{121'2'}, \quad (37)$$

where I_1 and I_2 represent the contributions of η_1 and η_2 in (32) and F , as above, denotes $F = f_1^0 f_2^0 (1 - f_1^0)(1 - f_2^0)$. In (37) we eliminated two integrals by integrating over a delta-function. Integrals I_3 and I_4 , which correspond to $\eta_{1'}$ and $\eta_{2'}$ respectively, can be written in a similar way:

$$I_3[\eta_k] = -A \int \frac{d^2 p_2 d\theta_{\mathbf{n}}}{(2\pi)^4} F_{121'2'} \eta_k(\mathbf{p}_{1'}), \quad (38)$$

$$I_4[\eta_k] = -A \int \frac{d^2 p_2 d\theta_{\mathbf{n}}}{(2\pi)^4} F_{121'2'} \eta_k(\mathbf{p}_{2'}). \quad (39)$$

In this case, eliminating integration over \mathbf{p}_2 by canceling it with the delta functions $\eta_k(\mathbf{p}_{1'})$, $\eta_k(\mathbf{p}_{2'})$ is a little more cumbersome. In the term I_4 the δ -function constraint is

$$\mathbf{p}_{2'}(\mathbf{p}_1, \mathbf{p}_2, \theta_{\mathbf{n}}) = \mathbf{k}, \quad (40)$$

where the expression for $\mathbf{p}_{2'}$ is given in (33). This equation should be solved for $\mathbf{p}_2(\mathbf{p}_1, \mathbf{k}, \theta_{\mathbf{n}})$, which is a zero of the δ -function's argument. To perform integration over \mathbf{p}_2 in (39) we use the value $\mathbf{p}_{1'}(\mathbf{p}_1, \mathbf{k}, \theta_{\mathbf{n}})$ and evaluate the Jacobian at the zero of the delta function. Conveniently, Eq. (40) can be solved in a closed form, after which the first relation in (33) yields

$$\mathbf{p}_2(\mathbf{p}_1, \mathbf{k}, \theta_{\mathbf{n}}) = 2\mathbf{k} - \mathbf{p}_1 - \frac{(\mathbf{k} - \mathbf{p}_1)^2 \mathbf{n}}{(\mathbf{k} - \mathbf{p}_1) \cdot \mathbf{n}} \quad (41)$$

$$\mathbf{p}_{1'}(\mathbf{p}_1, \mathbf{k}, \theta_{\mathbf{n}}) = \mathbf{k} - \frac{(\mathbf{k} - \mathbf{p}_1)^2 \mathbf{n}}{(\mathbf{k} - \mathbf{p}_1) \cdot \mathbf{n}}. \quad (42)$$

The Jacobian of a δ -function in I_4 is

$$J = \frac{(\partial p_{2'}^x, \partial p_{2'}^y)}{(\partial p_2^x, \partial p_2^y)} = \frac{1}{2} \frac{((\mathbf{k} - \mathbf{p}_1) \cdot \mathbf{n})^2}{(\mathbf{k} - \mathbf{p}_1)^2} \quad (43)$$

(found by linearizing the second relation in (33)). After handling the contribution I_3 in a similar manner, the sum of I_3 and I_4 can be simplified to read

$$(I_3 + I_4)[\eta_k] = -A \int \frac{d\theta_{\mathbf{n}}}{(2\pi)^4} J^{-1} F_{121'2'}, \quad (44)$$

where \mathbf{p}_2 and $\mathbf{p}_{1'}$ are given by Eqs.(41) and (42), and the Jacobian J is given by (43).

Importantly, evaluating I_2 , I_3 and I_4 on a delta function state, Eq.35, yields smooth functions of \mathbf{p} given by simple 1D integrals. The I_1 contribution, to the contrary, yields a delta function identical to the one in (35), with a prefactor that is given by a 3D integral. This contribution describes particle loss from the initial state \mathbf{p}_1 , the contributions I_2 , I_3 and I_4 describe gain.

One peculiar aspect of working with delta functions is a Jacobian that has a non-analytic structure, (43). We note that, while the Jacobian J is zero when condition $(\mathbf{k} - \mathbf{p}_1) \cdot \mathbf{n} = 0$ is satisfied, this does not mean that the whole expression inside the integral is divergent. The behavior of the integral around the divergent points of a phase space can be understood by introducing new variables Δp and ϕ , such that $\Delta p = |\mathbf{k} - \mathbf{p}_1|$ and $\cos \phi = (\mathbf{k} - \mathbf{p}_1) \cdot \mathbf{n} / \Delta p$. In these variables the Jacobian J can be written as

$$J = \cos^2 \phi, \quad (45)$$

an expression that remains finite and non-zero so long as $\cos \phi \neq 0$. Therefore, a divergence in the integral in (44) might occur only when the quantity $\cos \phi$ vanishes. On the other hand, expressions for \mathbf{p}_2 and $\mathbf{p}_{1'}$ in Eqs.(41) and (42) have a term $(\mathbf{p}_1 - \mathbf{k}) \cdot \mathbf{n}$ in their denominators, which is proportional to $\cos \phi$. Therefore at $\cos \phi = 0$ the absolute values of \mathbf{p}_2 and $\mathbf{p}_{1'}$ diverge so that $|\mathbf{p}_2| \rightarrow +\infty$ and $|\mathbf{p}_{1'}| \rightarrow +\infty$. This divergence leads to an exponential decrease of the $f(\mathbf{p}_2)$ term, which cancels the divergence of J^{-1} . Therefore, the expression inside the integral has only an isolated discontinuity point rather than a pole and therefore the integral has a finite value. Even though the integral is always integrable, the singularity near $\mathbf{p} = \mathbf{k}$ point makes the numerical computation problematic. We study the impact of the numerical error in forward scattering in the supplement and find out that it does not affect the qualitative behavior.

The representation of the collision operator introduced above can be used to project it on a subspace spanned by a set of basis functions chosen to provide a sufficiently good sampling of the active region in momentum space (the blurred annulus pictured in Fig.3). This yields a finite-size matrix that can be diagonalized to find the excitation eigenmodes and their eigenvalues, giving the decay rates. We have found that, although this direct approach works, it is more convenient to use a somewhat different approach to the problem, which employs the angular distribution of quasiparticle scattering in the active region near the Fermi surface.

The delta-function basis and an optimized integration mesh

Here we discuss the basis of functions in the momentum space used to represent particle momentum distributions perturbed by collisions. We describe the reasoning behind our basis choice and the integration mesh used in this study. In this work we opted for a basis comprised of suitably normalized delta functions. This choice is quite different from the more conventional approaches relying on systems of orthogonal polynomials (e.g. see [48]) The delta functions, being singular functions, may not appear to be a natural choice of a basis. However, in a problem like ours, the delta functions have distinct advantages, since, after being plugged in Eq.(10) of the main text they considerably reduce the number of required integrations.

As we observed, the nature of the δ -functions allows to eliminate two out of three integrations in three out of four terms in plugged in Eq.(eqnumber) of the main text. In addition, projection operation is effectively reduced to computing a value of the function of interest in the corresponding point, unlike in continuous functions bases, where we need to compute one more integral to perform the projection on the basis function itself. Additional complication comes from nature of the function inside the integral. At low temperatures it resembles several peaks in its variable space. This makes the Monte Carlo approach to the integration very hard to apply and pushes us to a mesh-based definite integration methods. Let us assume we perform the integration with M points in a mesh in momentum absolute value and with N mesh in angular variables. The computation time of the matrix element in continuous basis takes $O(M^2N^3)$ time. A non-diagonal element of the matrix, which is formed by only I_2 , I_3 , and I_4 , in some δ -function basis takes just $O(N)$ time. A diagonal element of a δ -function basis, where I_1 also has an impact, takes $O(MN^2)$. To solve a linear problem in a δ -function basis, we do not need to compute the matrix elements for each mesh point. As we show below, rotational symmetry of the initial expression allows us to perform the integration on M^2N mesh points instead of M^2N^2 for any non-diagonal matrix element and M points instead of MN points for diagonal elements. As takeaway, rotational symmetry of the initial expression allows to circumvent one of the integrations over θ . Therefore, the total computation complexity with the δ -function mesh is $O(M^2N^2)$ instead of $O(M^2N^3)$ for continuous bases.

With a very specific choice of a smooth basis for this particular problem it is possible to construct a numerical solution of a the same computational complexity. In particular, one needs to be rigorous in choosing the basis in the way that the choice would respect both rotational symmetry and properties of the integral. One of the possible ways to construct such basis is to use the form

$$f_{nm}(\mathbf{p}) = P_n(p)e^{im\theta}\tilde{F}(p), \quad (46)$$

where p and θ are polar coordinates of \mathbf{p} , $\tilde{F}(p) = f(1-f)$, and $P_n(p)$ is a polynomial of power n which is chosen to make $f_{nm}(\mathbf{p})$ to be orthogonal to $f_{n'm}(\mathbf{p})$ when $n \neq n'$ with respect to the integral inner product. This basis is one of the optimal bases, since it is both rotationally invariant and spans the region around the Fermi surface, but we stick to less complex basis of δ -functions.

Since computation of the collision integral on the delta-functions is much faster, we will use a sampling of delta-functions as a subspace basis for computation. We define a set of basis vectors as Kronecker δ -functions

$$|\mathbf{p}_i\rangle = \tilde{\delta}^{(2)}(\mathbf{p} - \mathbf{p}_i)\sqrt{\Delta V_i}, \quad (47)$$

where $\Delta V_i = p_i \Delta p_i \Delta \theta_i$; Δp_i and $\Delta \theta_i$ are sizes of the part of momentum space that corresponds to i 'th point in polar coordinates. By $\tilde{\delta}^{(2)}(\mathbf{p} - \mathbf{p}_i)$ in (47) we mean a function defined on the mesh and that is equal to 0 when $\mathbf{p} \neq \mathbf{p}_i$, and is equal to $1/\Delta V_i$ when $\mathbf{p} = \mathbf{p}_i$. In the limit of dense mesh function $\tilde{\delta}^{(2)}(\mathbf{p} - \mathbf{p}_i)$ behaves like a Dirac δ function. The square root of phase space element is added to preserve the normalization of the basis to be $\langle \mathbf{p}_i | \mathbf{p}_j \rangle = \delta_{ij}$ with respect to the inner product in the form of an integral over \mathbf{p} .

We use this basis to represent the operator I as a matrix:

$$\langle \mathbf{p}_i | I | \mathbf{p}_j \rangle \equiv I_{ij} = I[\tilde{\delta}^{(2)}(\mathbf{p}_i - \mathbf{p}_j)]\sqrt{\Delta V_i \Delta V_j}. \quad (48)$$

By this construction, the expression yields a symmetric matrix. As such it is suitable for computing the angular distribution for two-body scattering, for which the matrix should be applied to a state that represents the incoming state. It should be noted, however, that the eigenvectors and eigenvalues describing different excitations and their lifetimes are not those of the matrix I . Rather, they should be obtained from a generalized eigenvalue problem $\gamma \tilde{F}(p)|\psi\rangle = I|\psi\rangle$ with $\tilde{F}(p) = f_0(1-f_0)$.

On the side, the lowest eigenvalues for each m can be determined more easily from the angular distribution, as discussed in the main text. This approach was used to obtain the eigenvalues shown in Fig. 5 and Fig. 3 of the main text. We verified that the direct solution of the generalized eigenvalue problem gives the same eigenvalues, albeit with a lower accuracy.

Next, we discuss another crucial aspect of our analysis — sampling of the relevant part of the momentum space. This is achieved by constructing a mesh of points on which the delta-function states given in 47 are centered. The mesh must have a higher density near the Fermi surface and for near-collinear momenta, and also respect the cylindrical symmetry of the problem. There are several ways through which these requirements can be satisfied. Below we described the approach that proved particularly useful.

To preserve the rotational invariance of the collision operator, we take the the mesh points on a set of concentric circles centered at $\mathbf{p} = 0$, as illustrated in Fig.4. The radial momentum components form an equally spaced set of M points in an interval $p_{\min}(T) < p < p_{\max}(T)$ centered at $p = p_F$. To optimize coverage of the phase space within thermally broadened Fermi surface we used temperature dependence of $p_{\min}(T)$ and $p_{\max}(T)$ was optimized defined by $\tilde{F}(p_{\max}, T) = \tilde{F}(p_{\min}, T) = \alpha$, with $p_{\min} < p_{\max}$ and α a small parameter of choice. In this study we used several values of α and M and came to conclusion that the best choice that allows to achieve reasonable precision is $\alpha = 10^{-3}$ and $M = 40$. In cases when there was no lower-limit solution for $p_{\min} > 0$, the value p_{\min} was set to 0. The choice of boundaries on the absolute values of momentum in the mesh allows us to focus on the physically interesting region of the phase space near a Fermi surface where $\tilde{F}(\mathbf{p}, T)$ is not exponentially small. For the temperatures $T \sim \epsilon_F$, the sampled region was a disc of the radius $\sim \epsilon_F$. For the temperatures $T \ll \epsilon_F$, the sampled region was an annulus of radius ϵ_F and thickness of $\sim T$.

We choose a specific mesh point distribution to resemble the properties of the integral as a function of the angle between momenta \mathbf{p}_i and \mathbf{p}_j . To perform the collision operator analysis as a function of the angle, we need to be able to integrate over an absolute value of momentum (i.e. sum over points with the same angular coordinate and different radial coordinates). Because of this, we choose the same angular distribution of points for each circle of constant momentum absolute value. Assuming the δ -function source, we find that at low temperatures most of the scattering is either near-forward scattering or near-back scattering, and the width of the forward and backward peaks scales $\sim T$ at small temperatures. To describe this highly anisotropic scattering it is beneficial to define mesh that has a higher density for the angles in the near-forward and near-backward directions. To construct a mesh with such properties we choose a uniform mesh in angle to account for the general properties of the angular distribution. To that end, we use a combination of a uniform mesh for the angles away from the collinear and anticollinear directions $\theta = 0$ and π and a denser mesh concentrated in the regions near $\theta \approx 0$ and $\theta \approx \pi$. The width of these two regions is taken to be a function of temperature proportional to T , which accounts for the forward and backward scattering distribution becoming sharper as T decreases, as illustrated in Fig. 3 of the main text. The dense forward/backward mesh is taken to be uniform, comprised of N points. The not-so-dense mesh for non-collinear angles is also taken to be uniform, comprised of N' points. This is illustrated in Fig.4, where the dense and less dense meshes are shown in different colors. In our simulation we used $N = N' = 200$.

For a 2D mesh in momentum space we use a direct product of the radial and angular meshes defined as described above. We denote the mesh points as $|\mathbf{p}_{mn}\rangle \equiv |p_m, \theta_n\rangle$, where $\mathbf{p}_{mn} = (p_m \cos \theta_n, p_m \sin \theta_n)$ and $1 < m < M$ and $1 < n < N + N'$.

Matrix representation of the linearized collision operator

Here we describe in details the method to obtain the angular distribution from the operator projected on the functional basis and show the correspondence of these operations to the operations with original collision integral in the function space.

We choose the source in the form of delta function in an angular space to describe the electron injection along $\theta = 0$. The radial distribution for injected electrons is chosen to be proportional to $-\partial f_0 / \partial \epsilon$. This corresponds to $\eta_0(p_i, \theta_j) \equiv \eta_0(\theta_j) = \delta(\theta - \theta_j)$ when $\theta_j = 0$. To focus on the angular part of the operator, we contract the matrix with a column corresponding to η_0 ; this is equivalent to integrating original expression over the radial coordinates of momenta:

$$\langle \theta_i | I | \theta_j \rangle \equiv \sum_{p, p', \theta, \theta'} \langle \eta_0(\theta_i) | p, \theta \rangle \langle p, \theta | I | p', \theta' \rangle \times \langle p', \theta' | \eta_0(\theta_j) \rangle \quad (49)$$

Here the summation over p is a summation over all values of p_m where $1 \leq m \leq M$, and summation over θ is a summation over all values of θ_n where $1 \leq n \leq N + N'$. The summation over p and θ in (49) corresponds to the integration over momentum space in the following way:

$$\sum_{p, \theta} \langle \eta_0(\theta_i) | p, \theta \rangle \langle p, \theta | I | p_m, \theta_n \rangle \leftrightarrow \int_0^{+\infty} dp p \int_0^{2\pi} d\theta \eta_0(\theta_i) I[\delta^{(2)}(\mathbf{p} - \mathbf{p}_{mn})], \quad (50)$$

Analogous relations can be established for summations over p' and θ' .

Note that $\langle \theta_i | I | \theta_j \rangle$ depends only on the angles and does not depend on the absolute values of two momenta anymore. This happened because we assumed that the source of the injected electrons has $-\partial f / \partial \epsilon$ profile, and we also projected it onto a $-\partial f / \partial \epsilon$ state. We use this model because we are mainly interested in the decay of the "near ground state" modes of Eq. 8 in the main text, which is exactly proportional to $-\partial f / \partial \epsilon$ state. The angular distribution of scattered particles $\sigma(\theta_i)$, is obtained by setting $\theta_j = 0$:

$$\sigma(\theta_i) = \langle \theta_i | I | 0 \rangle, \quad (51)$$

The distribution $\sigma(\theta)$ is shown in Fig. 3 of the main text.

Initial operator $I[\delta(\mathbf{p} - \mathbf{k})](\mathbf{p}_1)$ has a rotational symmetry in a sense that the integral is only a function of $k = |\mathbf{k}|$, $p_1 = |\mathbf{p}_1|$, and an angle in-between \mathbf{p}_1 and \mathbf{k} . Consequently, the matrix elements $\langle \theta_i | I | \theta_j \rangle$ depend only on the $(\theta_i - \theta_j)$ combination: $\langle \theta_i | I | \theta_j \rangle = G(\theta_i - \theta_j)$. The eigenvalues of such a matrix are readily obtained by applying a discrete Fourier transform to $G(\theta)$. Therefore, the eigenvalues of the operator $\langle \theta_i | I | \theta_j \rangle$ can be obtained in the matrix notation by transforming $\sigma(\theta)$ as

$$\lambda_m = \sum_i e^{-im\theta_i} \sigma(\theta) \Delta\theta_i. \quad (52)$$

The quantity $\sigma(\theta_i)$ has the meaning of the transition rate per unit angle, with the dimensionality of $\text{sec}^{-1} \text{rad}^{-1}$. The dependence $\sigma(\theta)$ is constrained by particle conservation

$$\sum_i \Delta\theta_i \sigma(\theta_i) = 0 \quad (53)$$

and momentum conservation

$$\sum_i \Delta\theta_i \cos \theta_i \sigma(\theta_i) = \sum_i \Delta\theta_i \sin \theta_i \sigma(\theta_i) = 0. \quad (54)$$

in two-body collisions. These constraints yield the identities

$$\lambda_0 = \lambda_1 = 0. \quad (55)$$

The accuracy with which these relations hold provides a useful check for the precision of our numerical method. As an illustration, the eigenvalue λ_1 is shown in Fig. 1 of the main text (dashed curve). In general $\sigma(\theta)$ is a sign-changing function, with $\sigma(\theta) < 0$ corresponding to the emission of holes in the backward direction. This behavior is illustrated in Fig. 3 of the main text.

On the side, because of the rotational symmetry we do not need to compute all the entries of the matrix $\langle p_m, \theta_n | I | p_{m'}, \theta_{n'} \rangle$. For our purpose it is sufficient to evaluate the vector $\langle p_m, \theta_n | I | p_{m'}, 0 \rangle$, a quantity that for a rotationally invariant problem contains all the information about the operator and its eigenvalues. Therefore, the computation complexity of the problem is reduced from being quadratic in the number of angular points N to that linear in N , while remaining quadratic in the number of radial points M .

Separating contributions of the backscattering and forward scattering processes

In this subsection we describe the method of separation of the backscattering from more noisy forward scattering and show that the details of forward scattering has no significant impact on the backscattering. We use this method to show that the potential numerical problems of our approach described above do not affect the qualitative features of the back-scattering and the eigenvalue hierarchy of odd and even harmonics. The initial assumption about the absolute value of the scattering matrix element in $|V| = \text{const}$. Due to computational problems with precision of the forward scattering, we wish to study a modified potential that would prevent particles from scattering in a forward direction while keeping the backscattering effect intact. To accomplish this we choose a new 2-particle scattering potential that would satisfy $|V| \approx 0$ in the vicinity of $\mathbf{p}_1 \approx \mathbf{p}'_1$ and $\mathbf{p}_1 \approx \mathbf{p}'_2$ points. An example of a function that approaches zero when some $\mathbf{p}_1 \approx \mathbf{p}'_1$ is

$$g(\mathbf{p}_1 - \mathbf{p}'_1) = (1 - \exp[-(\mathbf{p}_1 - \mathbf{p}'_1)^2 / a^2]). \quad (56)$$

We consider 4 values of $a = 1, 1/2, 1/4, 1/8$ to study eigenvalue dependence on the cutoff parameter a . To make the scattering matrix element to be explicitly symmetric under the time reversal symmetry and particle permutations, we construct it in a following way:

$$w(\mathbf{p}_1, \mathbf{p}_2, \mathbf{p}'_1, \mathbf{p}'_2) \sim |V|^2 g(\mathbf{p}_1 - \mathbf{p}'_1) g(\mathbf{p}_1 - \mathbf{p}'_2) g(\mathbf{p}_2 - \mathbf{p}'_1) g(\mathbf{p}_2 - \mathbf{p}'_2) \quad (57)$$

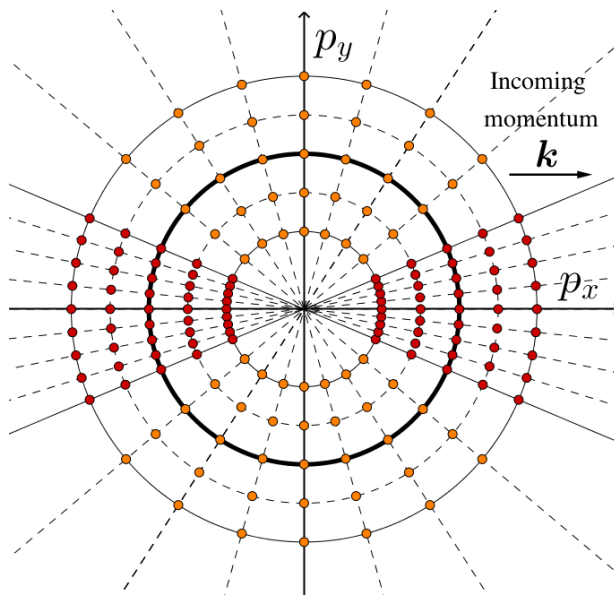


FIG. 4. The mesh in momentum space used in the calculation. The mesh density is nonuniform to achieve better coverage of angles for the collinear and anti-collinear directions relative to the incoming momentum \mathbf{k} . This choice guarantees that the mesh respects rotational symmetry of the problem. In the actual calculation we used $M = 40$ radial points, $N = 200$ azimuthal points for a less dense mesh (orange points), and $N' = 200$ points for a more dense mesh in the collinear and anti-collinear direction of \mathbf{k} (red points). Accordingly, the total numbers of angles in the collinear and anti-collinear groups was $N'/2$; the total number angles in the non-collinear upper and lower groups was $N/2$. The radial mesh was chosen to span an annulus covering the Fermi surface (marked by a bold circle). To account for the strong collinear and anti-collinear contributions in the two-body scattering, the x, y coordinates are rotated so that the x axis is aligned with the incoming momentum \mathbf{k} .

instead of $w(\mathbf{p}_1, \mathbf{p}_2, \mathbf{p}'_1, \mathbf{p}'_2) \sim |V|^2$. We use the properly normalized scattering probability element from (57) with other parameters including temperature, integration mesh, and numerical integration precision being the same. This calculation repeats all the steps of the main calculation, but takes the transition element to approach zero in the case of forward scattering, which effectively turns it off and allows to omit the singularity during numerical integration of Eq. 21 of the main text.

The plot of backscattering $\sigma(\theta)$ analogous to Fig. 3 of the main text is shown in Fig. 5. The backscattering with separated forward scattering in Fig. 5 resembles the same qualitative properties as the backscattering in Fig. 3 of the main text while showing better numerical results and more abrupt regime change. The distribution enters the low-temperature scaling regime faster: the angular distribution already reaches T^2 scaling in the amplitude at the temperature $T = 0.32 T_F$, which can be observed at Fig. 5.

The deviation in behavior of the eigenvalues of odd m harmonics from the behavior of eigenvalues of even m harmonics shows up at the temperatures lower than $T = 0.32 T_F$, its behavior can be seen in Fig. 6. Besides the absence of the forward scattering, such calculation produced result analogous to the main results, which means that the forward scattering plays little role in creating the hierarchy of eigenvalues.

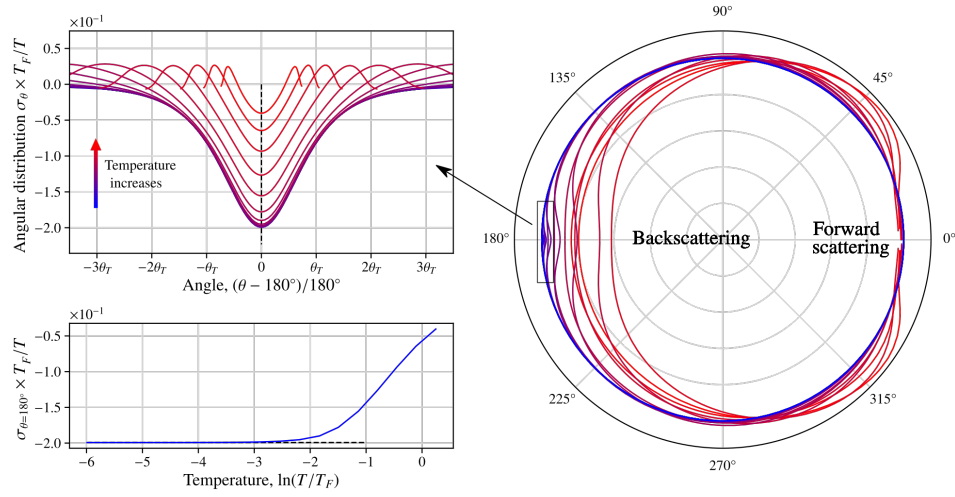


FIG. 5. Angular distribution $\sigma(\theta)$ of scattered particles for different temperatures calculated for a potential that effectively separates forward scattering. The temperatures used in this plot are $T/T_F = 0.0025, 0.005, 0.01, 0.02, 0.04, 0.08, 0.16, 0.32, 0.64, 1.28$. The value of the coefficient used in (57) is $a = 1/2$.

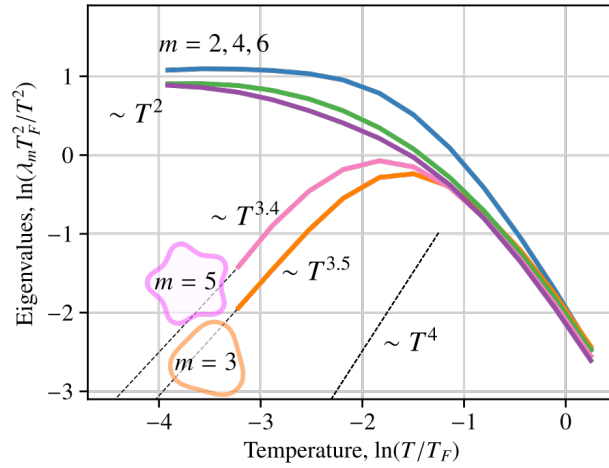


FIG. 6. Eigenvalues for different harmonics as a function of temperature. Even m eigenvalues show the T^2 scaling with temperature already at $T = 0.16T_F$. Odd eigenvalues start to diverge from T^2 scaling to faster scaling regimes at temperatures lower than $T = 0.32T_F$. The back-scattering shows T^2 dependence in the intensity σ and T dependence of the width of the scattering peak.